Macromolecules
ARTICLE

Macromolecules **2010**, *43*, 7657–7667 **7657**
DOI: 10.1021/ma101549z

Thermally Rearranged (TR) Polybenzoxazole: Effects of Diverse Imidization Routes on Physical Properties and Gas Transport Behaviors

Sang Hoon Han,[†] Nurasyikin Misdan,[†] Seungju Kim,[†] Cara M. Doherty,[§] Anita J. Hill,[§] and Young Moo Lee*[,†,‡]

[†]*School of Chemical Engineering, College of Engineering, Hanyang University, Seoul 133-791, Republic of Korea,* [‡]*WCU Department of Energy Engineering, College of Engineering, Hanyang University, Seoul 133-791, Republic of Korea, and* [§]*Commonwealth Scientific and Industrial Research Organization (CSIRO), Private Bag 33, Clayton South, Victoria 3169, Australia*

Received July 19, 2010; Revised Manuscript Received August 19, 2010

ABSTRACT: Conversion of hydroxyl-containing polyimides into polybenzoxazole can be achieved by thermal rearrangement of the aromatic polymer chain with decarboxylation at elevated temperature. Synthetic methods to prepare polyimide precursors are important for the resulting thermally rearranged (TR) polymer membranes. Here, we report on the effect of several imidization methods on the properties of TR polymer membranes. Thermal and chemical imidizations are the most common routes to prepare polyimides, and solution thermal imidization using an azeotrope is also widely used, especially to obtain soluble polyimide-containing functional groups. We report here on the syntheses of ortho-functional polyimides from 4,4′-hexafluoroisopropylidene diphthalic anhydrides and 2,2′-bis(3-amino-4-hydroxyphenyl)hexafluoropropane by three different imidization methods. Acetate-containing polyimides by chemical imidization and further silylation treatment as well as hydroxyl-containing polyimides by thermal and azeotropic imidization are characterized using thermogravimetric analysis, density, positron annihilation lifetime spectroscopy, and gas permeation property measurements. Comparison between the precursor polyimides and the resulting thermally rearranged polybenzoxazole (TR-PBO) membranes exhibited significant increase in fractional free volumes and cavity sizes followed by enhanced gas permeation properties.

Introduction

Polyimide is a glassy polymer exhibiting excellent properties such as thermal and mechanical stability, chemical and radiation resistance, good processability and adhesion properties, a low dielectric constant, low relative permittivity, and long-term stability.[1,2] Since being first reported in 1908 and followed by the introduction of the high molecular weight polyimide in the 1950s, polyimides have played important roles in electronics, aerospace insulators, adhesives, photoresists, nonlinear optical materials, and separation membranes.[1,3] Polyimide-based membranes have been applied in reverse osmosis (RO), microfiltration (MF), ultrafiltration (UF), pervaporation (PV), and gas separation (GS).[4] In particular, gas separation by polyimide membranes has shown very promising permeabilities and selectivities because polyimides are composed of rigid main chains with strong intermolecular interactions, which result in very small sizes and low intensities in free volume.[2]

Diffusion and sorption characteristics, as well as gas permeabilities and structure−property relationships of various polyimide membranes, have been extensively investigated containing plasticization, humidification, and cross-linking effects.[5−8] The variation in structure−property relationships of polyimide membranes due to different types of substitution groups in the main chain and side chain have been summarized empirically, relative to molar volume, density, free volume, and gas permeabilities by means of group contribution theory.

Structure-modified polyimides have been reported to obtain optimized properties for specific separation targets. Chung and co-workers developed a cross-linked polyimide membrane which is constructed with an amide−imide network for enhanced H_2/CO_2 separation.[9,10] Impregnation of aliphatic diamine cross-linkers broke imide domains and altered them into a cross-linked structure to control polymer flexibility and free volume elements. Flexible and bulky polyimides containing fluorene moieties were also synthesized to obtain distorted stiff structures, and the resulting high free volume elements were similar to polymers with intrinsic microporosity (PIMs).[11,12] Furthermore, instead of the chemically stable alkyl chains, polyimide-containing functional groups in the side chain were also synthesized and investigated by introducing hydroxide, carboxylic acid, and sulfonic acid moieties. Okamoto and co-workers prepared hydrophilic polyimides as well as hyperbranched polyimides for olefin/paraffin separation, fuel cells, and precursors for carbon membranes for gas separation.[13,14] Hydrophilicity in polyimides affects the physical properties due to increased hydrogen bonds and intermolecular interactions and can also provide cross-linking or grafting sites.[15−17]

Physical properties of these numerous polyimides were affected by the imidization methods. To synthesize polyimide membranes, thermal and chemical imidization methods have been commonly used via a two-step reaction of poly(amic acid) (PAA) intermediate from dianhydride and diamine monomers. Thermal imidization is a method which induces endothermic ring closure by dehydration during thermal treatment up to 300 °C while chemical imidization is performed by the chemical reaction of acetic anhydride with an amic acid moiety followed by the elimination of acetic acid under basic conditions provided by pyrridine or triethylamine at room temperature.[18] Compared with chemical imidization, where the chemical reagent reacts with PAA, solution thermal imidization, or what is known as azeotropic imidization, uses a solvent that forms

*Corresponding author: Tel +82-2-2220-0525; Fax +82-2-2291-5982; e-mail ymlee@hanyang.ac.kr.

Published on Web 09/01/2010

an azeotrope with H_2O (such as benzene or toluene), which can be used to evaporate water in the form of this azeotropic mixture from the PAA solution, resulting in dehydration and imidization around 160 °C. These diverse imidization routes, therefore, can affect the polyimides with respect to their chemical structure, solubility, and physical and transport properties.[19] Furthermore, pretreatment of monomers by adding chlorotrimethylsilane (CTMS) also improves the properties of polyimides, since silylation, which makes the diamine more nucleophilic, contributes to an increase in the molecular weight far above that obtained for polyimides prepared from the pristine diamine.[20,21]

Thus, imidization methods can also affect the properties and performances of polyimide derivatives. The formation of thermally rearranged (TR) polymers obtained from polyimides with ortho-functional groups (PIOFGs) is dependent upon the imidization routes as well. Because the ortho-functional groups in polyimide attack the imide domain and result in the conversion of the polymer structure, thermal treatment of PIOFG and the following decarboxylation at elevated temperature yields highly rigid heteroaromatic polymers such as polybenzoxazole (PBO), polybenzothiazole (PBT), polypyrrolone (PPL), and polybenzimidazole (PBI).[22,23] Solid-state rearrangement by heat treatment was shown to affect the topologies and the intrinsic properties of TR polymers and resulted in unusual increases in free volume elements as well as extraordinarily high gas permeation properties.[24]

Here, we prepared and characterized PBO membranes by thermal rearrangement of hydroxyl-containing polyimides (HPIs) and acetate-containing polyimides (AcPIs) via diverse imidization methods (thermal, azeotropic, chemical imidization, and further silylation treatment) to elucidate the effect of imidization route on the properties of precursor PIs and the resultant TR-PBO membranes for a given thermal treatment condition.

Experimental Section

Materials. To prepare polybenzoxazoles via four imidization procedures, high-purity (99.9+%) 4,4′-hexafluoroisopropylidene diphthalic anhydride (6FDA) (Scheme 1, **1**) and 2,2-bis(3-amino-4-hydroxyphenyl)hexafluoropropane (bisAPAF) (**2**) were purchased from Daikin Industries, Ltd. (Osaka, Japan) and Central Glass Co. Ltd. (Tokyo, Japan), respectively. The monomers were dried at 160 and 120 °C under reduced pressure for 12 h before use. *N*-Methyl-2-pyrrolidinone (NMP), *o*-cresol, pyridine, and chlorotrimethylsilane (CTMS), used as solvents and catalysts, were obtained from Aldrich Chemical Co. (Milwaukee, WI) and were used without further treatment.

Poly(amic acid)s (3). All pretreated chemicals and glassware were put in a globe box and purged with dried nitrogen to prevent monomers from reacting with water vapor. BisAPAF (10 mmol) as a diamine was dissolved in a 250 mL three-neck round-bottomed flask filled with NMP (32 mL). After stirring for 1 h under nitrogen atmosphere, 6FDA (10 mmol) was slowly added to the solution and stirred 3 h in an ice bath, inducing a spontaneous ring-opening reaction of dianhydride with diamine. This yielded a yellowish hydroxyl-containing poly(amic acid) (HPAA) (**3**) solution.

Hydroxyl-Containing Polyimide (HPI) by Thermal Imidization (4a, tHPI). The intermediate HPAA solution was degassed at room temperature, cast onto a glass plate, and thermally imidized in a vacuum oven. It was heated to 60, 100, 150, 200, and 250 °C for 1 h at each isothermal step, and a polyimide film was formed by solvent evaporation. The film was detached from the glass plate, washed, dried overnight at 120 °C, and thermally treated to complete the thermal ring-closure reaction up to 300 °C in a muffle furnace. FT-IR (film): ν(−OH) at 3369 cm^{-1}, imide ν(⟩C═O) at 1786 and 1716 cm^{-1}, imide ν(C−N) at 1377 cm^{-1}. T_g (DSC) 301 °C; average *d*-spacing 0.57 nm; density 1.47 g cm^{-1}; fractional free volume (FFV) 0.19.

Scheme 1. Preparation of Polybenzoxazoles via Polyimides: (1) 4,4′-Hexafluoroisopropylidene Diphthalic Anhydride, (2) 2,2′-Bis(3-amino-4-hydroxyphenyl)hexafluoroisopropylidene, (3) Hydroxyl-Containing Poly(amic acid) (HPAA), (4a,b) Hydroxyl-Containing Polyimide (HPI), (4c,d) Acetate-Containing Polyimide (AcPI), (5a−d) Polybenzoxazole (PBO)

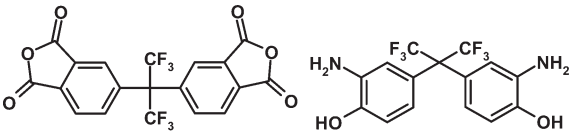

1 2

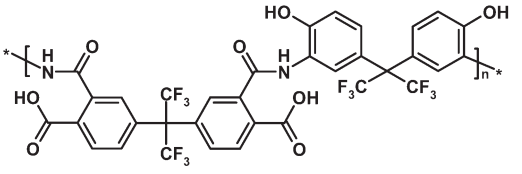

3

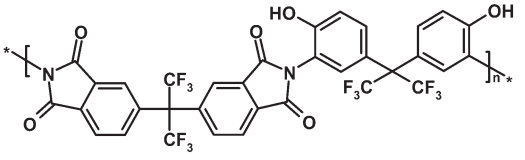

4a (tHPI), 4b (aHPI)

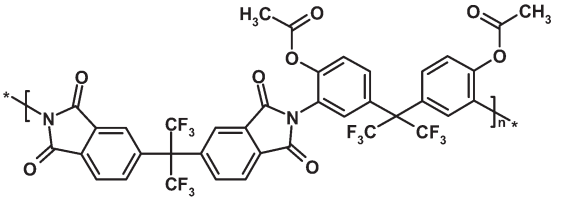

4c (cAcPI), 4d (sAcPI)

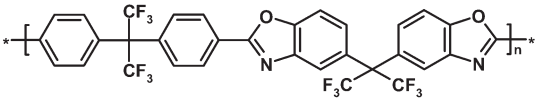

5a (tPBO), 5b (aPBO), 5c (cPBO), 5d (sPBO)

Hydroxyl-Containing Polyimide (HPI) by Azeotropic Imidization (4b, aHPI). The round-bottomed flask containing intermediate HPAA (**3**) solution in NMP was moved into an oil bath with a temperature controller and connected to a Dean-Stark trap with a water-circulated condenser. *o*-Xylene (30 mL) as an azeotropic agent was added to the solution, which was stirred vigorously and heated. The oil bath was heated slowly to 180 °C and was maintained for 6 h for solution imidization over which time the water/*o*-xylene azeotrope mixture was fully evaporated and condensed. The resulting brown solution was cooled to room temperature, precipitated in distilled water, and then dried in a convection oven at 150 °C for 12 h. ^{1}H NMR (300 MHz, DMSO-d_6): 10.41 (s, 2 H, OH), 8.10 (d, 2 H, J = 8.0 Hz), 7.92 (d, 2 H, J = 8.0 Hz), 7.71 (s, 2 H), 7.47 (s, 2 H), 7.20 (d, 2 H, J = 8.3 Hz), 7.04 ppm (d, 2 H, J = 8.3 Hz). FT-IR (film): ν(−OH) at 3371 cm^{-1}, imide ν(⟩C═O) at 1786 and 1716 cm^{-1}, imide ν(C−N) at 1377 cm^{-1}. Molecular weight: M_w = 81 688, M_n = 24 297 with a polydispersity of 3.4; T_g (DSC) 301 °C; average *d*-spacing 0.54 nm; density1.49 g cm^{-1}; fractional free volume (FFV) 0.17.

Acetate-Containing Polyimide (AcPI) by Chemical Imidization (4c, cAcPI). Intermediate HPAA (**3**) dissolved in NMP was mixed with excess acetic anhydride (4.7 mL) and pyridine (4.0 mL) and was stirred vigorously for chemical imidization at room temperature and 12 h. The product was precipitated in distilled water and dried in a convection oven at 150 °C and 24 h.

^{1}H NMR (300 MHz, DMSO-d_6): 2.12 (s, 6 H, CH_3), 8.15 (d, 2 H, J = 8.0 Hz), 7.93 (d, 2 H, J = 8.0 Hz), 7.79 (s, 2 H), 7.77 (s, 2 H), 7.56 (d, 2 H, J = 8.5 Hz), 7.46 ppm (d, 2 H, J = 8.5 Hz). FT-IR (film): imide ν(⟩C═O) at 1784 and 1726 cm^{-1}, imide ν(C−N) at 1373 cm^{-1}; molecular weight: M_w = 81 758, M_n = 40 787 with a polydispersity of 2.0; T_g (DSC) 265 °C; average d-spacing 0.59 nm; density 1.45 g cm^{-3}; fractional free volume (FFV) 0.18.

Acetate-Containing Polyimide (AcPI) by Chemical Imidization with Silylation Treatment (4d, sAcPI). The synthetic procedure of sAcPI was performed as cAcPI above except that 40 mmol of CTMS was added and reacted for 3 h with bisAPAF before preparing HPAA to activate the diamine monomer by silylation. ^{1}H NMR (300 MHz, DMSO-d_6): 2.12 (s, 6 H, CH_3), 8.15 (d, 2 H, J = 8.0 Hz), 7.93 (d, 2 H, J = 8.0 Hz), 7.80 (s, 2 H), 7.77 (s, 2 H), 7.57 (d, 2 H, J = 8.5 Hz), 7.46 ppm (d, 2 H, J = 8.5 Hz); FT-IR (film) imide ν(⟩C═O) at 1782 and 1728 cm^{-1}, imide ν(C−N) at 1373 cm^{-1}; molecular weight: M_w = 95 914, M_n = 23 903 with a polydispersity of 4.0; T_g (DSC) 268 °C; average d-spacing 0.60 nm; density 1.42 g cm^{-3}; fractional free volume (FFV) 0.19.

Film Formation and Thermal Conversion to Polybenzoxazoles. To prepare polyimide films (except the thermally imidized polyimide, which was cast before imidization), 15 wt % polyimide solutions in NMP were filtered with a 0.2 μm Teflon syringe filter and cast onto clean glass plates. Cast films were placed in a vacuum oven and heated slowly to 250 °C with holds for 1 h at 100, 150, and 200 °C to evaporate the solvent under high vacuum. The solid films were taken off the glass plates, rinsed with deionized water, and dried at 120 °C until the residual solvent and water were removed. The defect-free and clean membranes (samples **4a** to **4d**) were cut into 3 cm × 3 cm size strips and placed between quartz plates to prevent film deformation at elevated temperature in a muffle furnace. Each sample was heated to 300 °C at a rate of 5 °C/min, held for 1 h to eliminate residual solvent, heated further to 450 °C, and maintained for 1 h in a high-purity argon atmosphere. After thermal treatment, the furnace was slowly cooled to room temperature, and the brown membranes were stored in a desiccator.

Polybenzoxazole derived from HPI via thermal imidization (tPBO, **5a**): average d-spacing 0.64 nm; density 1.27 g cm^{-3}; fractional free volume (FFV) 0.28.

Polybenzoxazole derived from HPI via azeotropic imidization (aPBO, **5b**): average d-spacing 0.58 nm; density 1.38 g cm^{-3}; fractional free volume (FFV) 0.22.

Polybenzoxazole derived from AcPI via chemical imidization (cPBO, **5c**): average d-spacing 0.67 nm; density 1.15 g cm^{-3}; fractional free volume (FFV) 0.35.

Polybenzoxazole derived from AcPI via chemical imidization with silylation (sPBO, **5d**): average d-spacing 0.75 nm; density 1.17 g cm^{-3}; fractional free volume (FFV) 0.33.

Measurements. Structural divergence between precursor polyimides was confirmed by ^{1}H NMR spectra obtained from a Varian Mercury Plus 300 MHz spectrometer (Varian, Inc., Palo Alto, CA) and Fourier-transformation infrared spectroscopy (FT-IR) from Magna-IR 760 ESP spectroscopy (Thermo Fisher Scientific Inc., Waltham, MA). Solid-state ^{13}C NMR (500 MHz, Bruker Avance II, Bruker Biospin Inc.) and elemental analysis (Thermofinnigan EA1108, Fisions Instrument Co., Italy) were introduced to prove the conversion of precursor polymer into polybenzoxazole. Molecular weights of soluble precursor polyimides were measured by gel permeation chromatography (GPC, Tosoh HLC-8320 GPC, Tokyo, Japan) with a TSK SuperMultipore HZ-M column and a refractive index (RI) detector in THF on the basis of standard polystyrenes. Glass transition temperatures (T_g) were obtained by DSC Q20 (TA Instruments, New Castle, DE) at a rate of 5 °C/min from 100 to 350 °C for precursors or to 500 °C for polybenzoxazoles. Thermal properties of precursors using thermogravimetric analysis (TGA) with mass spectroscopy (MS) were investigated to confirm thermal rearrangement and the resulting byproduct gases by TGA Q500 (TA Instruements, New Castle, DE) at a rate of 10 °C/min with ThermoStar GSD 301T (Pfeiffer Vacuum GmbH, Asslar, Germany). Wide-angle X-ray diffractometry (WAXD) (Rigaku Denki D/MAX-2500, Rigaku, Japan) proved intermolecular distance of PI precursors and PBO membranes via the d-spacing value obtained from Bragg's equation in the 2θ range of 5°−50° with a scan rate of 5°/min by 1.54 Å wavelength of Cu Kα radiation source. Sorption characteristics by nitrogen at 77 K were observed by a surface area and porosimetry analyzer (ASAP 2020, Micromeritics Instrument Corp., Norcross, GA) after degassing of finely ground samples at 300 °C for 6 h. Fractional free volume (FFV, V_f), one of the most informative properties to understand the transport behavior through polymer membranes, was calculated from the densities measured by a Satorius LA 120S (Satorius AG, Goettingen, Germany) balance with a density kit by a buoyancy method as follows:

$$V = \frac{M_0}{\rho} \tag{1}$$

$$V_f = \frac{V - 1.3V_w}{V} \tag{2}$$

where V is the molar volume of polymers (mol cm^3/mol) derived from the density and V_w is the van der Waals molar volume based on Bondi's group contribution theory.

Positron annihilation lifetime spectroscopy (PALS) was used to determine the size distribution and relative intensity of free volume elements within the polymer membranes and allows an investigation into the transport mechanism of small gases and ions. Positrons emitted from a radioactive ^{22}Na source thermalize within the sample. The positrons can form two bound states with electrons known as positronium (Ps): o-Ps is the parallel spin combination and p-Ps has antiparellel spins. Self-annihilation of p-Ps and free annihilation (positron annihilation with an electron within the sample) occur at 0.125 ns and ∼0.4 ns, respectively. Pick-off annihilation of o-Ps in a molecular system is affected by the electron density in the surroundings. That is, the o-Ps can survive longer in a system or local domain with low electron density, such as pores, cavities, or free volume elements.[25,26] On the basis of the assumption that the vacant volume has a spherical shape, the measurement of the o-Ps lifetime (τ, ns) and its intensity (I, %) not only provide the size and distribution of free volume elements in the polymer but also shed light on the topologies in which different sized pores exist. PALS is able to distinguish the presence of bimodal porosity such as in highly microporous materials like PTMSP and PIM by fitting several o-Ps components.[27−30]

The size and distribution of free volume elements in the polymers was determined by PALS using an automated EG&G Ortec (Oak Ridge, TN) fast−fast coincidence spectrometer which had a resolution function of 230 ps fwhm peak when measured with ^{60}Co. The samples were composed of 10 mm × 10 mm size polymer films stacked to 1 mm in thickness with a ∼30 μCi ^{22}NaCl sealed Mylar source placed between the polymers. A source correction for the Mylar was required (1.6 ns, 3.12%). The samples were placed in a cell and subjected to a vacuum of 5 × 10^{-4} Pa at room temperature. The range of the time-to-amplitude converter (TAC) was extended to 200 ns to measure the long lifetimes, and the coincidence unit was removed to improve the count rates. A minimum of five files were collected with 1 × 10^6 integrated counts per file. The acquired data were analyzed using either a three- or four-component fit with the LTv9 software. The first lifetime (τ_1) was fixed to 0.125 ns due to p-Ps annihilation, and τ_2 was fitted to free annihilation (∼0.4 ns). The orthopositronium lifetimes (τ_3 and τ_4)

were used to calculate the free volumes within the membranes using the Tao−Eldrup equation

$$\tau_3^{-1} = 2\left[1 - \frac{r_3}{r_3 + \Delta r} + \frac{1}{2\pi}\sin\left(\frac{2\pi(r_3)}{r_3 + \Delta r}\right)\right] \quad (3)$$

where τ_3 is lifetime (ns), r_3 is cavity radius (Å), and Δr is determined empirically and is related to the thickness of the electron layer on the pore wall which interacts with the positronium (1.66 Å).[25]

Gas permeation properties as well as diffusion coefficients were obtained from a custom-made instrument using the time-lag method as described in our previous studies.[31] For six types of small gas molecules, He (2.6 Å), H_2 (2.89 Å), CO_2 (3.3 Å), O_2 (3.46 Å), N_2 (3.64 Å), and CH_4 (3.8 Å), the pressure was increased the membrane in a fixed downstream chamber from 0 to 10 mmHg against 760 mmHg of upstream pressure. In a steady state region of pressure as a function of time, the gas permeabilty coefficients can be calculated using the following equation:

$$P = \left(\frac{VT_0 l}{p_0 T \Delta p A}\right)\frac{dp}{dt} \quad (4)$$

where P (barrer) is the gas permeability, V (cm^3) is the downstream volume, l (cm) is the membrane thickness, Δp (cmHg) is the pressure difference between upstream and downstream, T (K) is the measurement temperature, A (cm^2) is the effective membrane area, p_0 and T_0 are the standard pressure and temperature, and dp/dt is the rate of the pressure rise at steady state. The ideal selectivity ($\alpha_{1/2}$) for components 1 and 2 was defined as the ratio of the gas permeabilities of the two components.

Results and Discussion

Preparation of Precursor Polyimides. For comparison of thermally rearranged polybenzoxazole membranes from ortho-functional polyimide, four imidization methods were employed: (a) thermal imidization, (b) azeotropic imidization, (c) chemical imidization, (d) chemical imidization with silylation pretreatment. To synthesize functional polyimides, the polyimides containing a hydroxyl or acetate group were prepared from 6FDA dianhydride (**1**) and bisAPAF diamine (**2**) by a two-step method via hydroxyl poly(amic acid) (**3**). Thermal imidization is a common imidization method, which is performed by heating the intermediate poly(amic acid) and evolving H_2O followed by ring closure to imides, which occurs above 200 °C. At this temperature, a polar aprotic solvent like NMP is evaporated along with water accompanied by a substantial thermal cross-linking of poly(amic acid) as well as intramolecular dehydration imidization. Therefore, the resulting polyimide, e.g., tHPI (**4a**), has very poor solubility in common organic solvents (Table 1).

While thermal imidization takes place with an evaporation of solvents, azeotropic imidization occurs in solution by adding reagents to form azeotropes with water during the reaction. At a mild reaction temperature around 140−180 °C, the azeotropic imidization method may result in a soluble polyimide due to the intramolecular interaction if the main chain of the polyimide is flexible enough to be dissolved in organic solvents. Accordingly, by the imidization of 6FDA and bisAPAF monomers, soluble hydroxylpolyimide (aHPI, **4b**) was prepared successfully. Because of the bulky hexafluoroisopropylidene moieties in dianhydride and diamine monomers, polymer **4b** was soluble in polar aprotic solvents such as NMP, DMSO, DMF, and THF (Table 1). Furthermore, the hydrophilic −OH group in the main chain induced polymer solublity even in ethanol and methanol.[32,33] The weight-average molecular weight and polydispersity of **4b** by GPC were 81 688 and 3.4, respectively.

Table 1. Solubilities of Precursor Polyimides in Common Organic Solvents

	solubility in organic solvent			
solvent[a]	HPI from thermal imidization (tHPI, **4a**)	HPI from azeotropic imidization (aHPI, **4b**)	AcPI from chemical imidization (cAcPI, **4c**)	AcPI from chemical imidization with silylation method (sAcPI, **4d**)
NMP	−	++	++	++
DMAc	−	++	++	++
DMSO	−	++	++	++
THF	−	++	++	++
acetone	−	++	++	++
MeOH	−−	+	−−	−−
EtOH	−−	+	−−	−−
IPA	−−	+	−	−
EG	−−	−	−	−

[a] NMP: *N*-methylpyrrolidinone; DMAc: *N,N*-dimethylacetamide; DMSO: dimethyl sulfoxide; THF: tetrahydrofuran; MeOH: methanol; EtOH: ethanol; IPA: 2-propyl alcohol; EG: ethylene glycol.

Chemical imidization of monomers is of interest; however, HPI could not be prepared via this method even though it is commonly used to prepare soluble polyimides. In this method, where chemical reaction of amic acid and acetic anhydride was conducted prior to the elimination of acetic acid at room temperature, the highly reactive acetic anhydride attacked the hydroxyl group in the diamine moiety as well as the carboxylic acid in the main chain of the poly(amic acid). Without any protecting group, the hydroxyl group of bisAPAF was substituted to create an acetate group, and the acetate-containing polyimide (cAcPI, **4c**) was obtained. The weight-average molecular weight and polydispersity of **4c** were 81 758 and 2.0, respectively.

Combined with the chemical imidization method, silylation was introduced to obtain high molecular weight polymers. Silylation is a unique method to activate nucleophilic diamines and thus increase the reactivity of diamines. To prevent the highly reactive chlorotrimethylsilane from reacting with moisture, an in situ silylation was performed in which CTMS was added before the reaction of bisAPAF with 6FDA. Then, the synthesis of poly(amic acid silyl ester) followed the mechanism described in the literature.[20,21,34] Because the silylated amine and hydroxyl group undergo reduction during chemical imidization and precipitation in water, the silylation did not result in significant changes in comparison with pristine chemical imidization, except that the weight-average molecular weight of the acetate-containing polyimide increases from 81 758 (cAcPI, **4c**) to 95 914 (sAcPI, **4d**).

Characterization of the Precursor Polyimides. Three imidization methods and silylation should affect physical properties, including transport properties, solubility, molecular weight, and free volume elements in the polymer matrix. As confirmed by ATR-FT-IR and ^1H NMR spectroscopy, chemical structures of the polyimides were dependent upon whether the diamine monomer reacted with additives during the imidization procedure. In ATR-FT-IR spectra (as shown in Figure 1), no substantial peaks around 3400 cm^{-1} in **4c** and **4d** were observed, which is consistent with the substitution of hydroxyl group for an acetate group. However, **4a** and **4b** exhibited clear hydroxyl groups at 3369 and 3371 cm^{-1}. Moreover, the characteristic imide group bands near 1716 cm^{-1} in HPIs shifted to 1726 and 1728 cm^{-1} in AcPIs due to the electron-withdrawing effect of the acetate group.

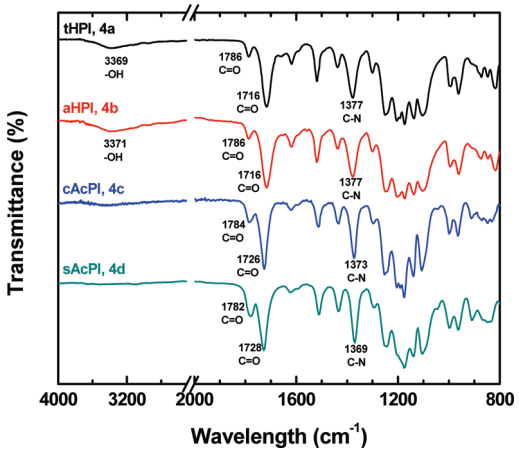

Figure 1. ATR-FT-IR spectra of precursor polyimides.

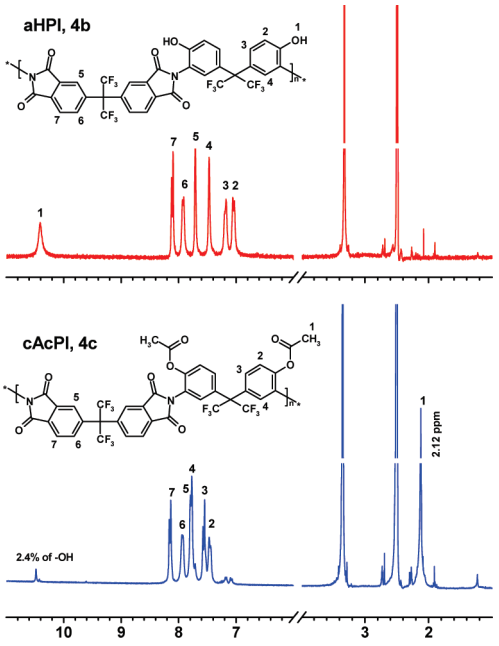

Figure 2. ^{1}H NMR (DMSO-d_6, 300 MHz) spectra of precursor polyimides.

Table 2. Physical Properties of Precursor Polyimides and Polybenzoxazoles

	density (g/cm^3)	molar volume (g/cm^3)	fractional free volume (FFV)	increment in FFV (%)	*d*-spacing (nm)
tHPI, **4a**	1.47	0.687	0.19	48	0.57
tPBO, **5a**	1.27	0.788	0.28		0.64
aHPI, **4b**	1.49	0.673	0.17	29	0.54
aPBO, **5b**	1.38	0.727	0.22		0.58
cAcPI, **4c**	1.45	0.690	0.18	96	0.59
cPBO, **5c**	1.15	0.873	0.35		0.67
sAcPI, **4d**	1.42	0.704	0.19	73	0.60
sPBO, **5d**	1.17	0.855	0.33		0.75

^{1}H NMR (Figure 2) spectra of **4b** exhibited strong aromatic hydroxyl resonances at 10.4 ppm. Aromatic hydrogens in bisAPAF moieties corresponded to 7.05, 7.17, and 7.47 ppm while aromatic hydrogen peaks in 6FDA moiety were found slightly downfield (7.71, 7.91, and 8.10 ppm) due to the deshielding of ring current effects of π-bonds in the conjugated imide domain.[35] The spectrum of **4c**, on the other hand, showed more complicated patterns, assuming that there is a mixture of hydroxyl−polyimide and acetate−polyimide. Acetate groups in the side chain should show a strong methyl hydrogen peak at 2.12 ppm[36] and also should affect the shift of aromatic hydrogen peaks. As aromatic hydrogens in the 6FDA moiety were detected at 7.78, 7.93, and 8.13 ppm, hydrogens adjacent to the acetate group were deshielded distinctively to 7.45, 7.55, and 7.58 ppm. However, a small quantity of residual hydroxyl group was found at 7.07, 7.17, and 10.8 ppm, indicating that the reaction of acetic anhydride with hydroxide was not performed completely during chemical imidization at room temperature.

Depending on the synthetic methods, the fluorinated polyimides showed distinctive physical properties (Table 2),

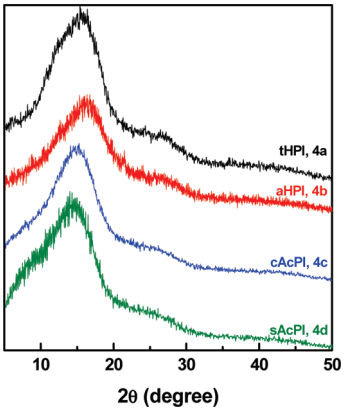

Figure 3. Wide-angle X-ray diffraction (WAXD) patterns of precursor polyimides.

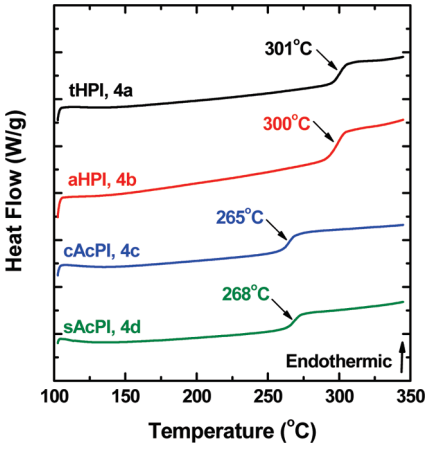

Figure 4. Glass transition temperature of precursor polyimides.

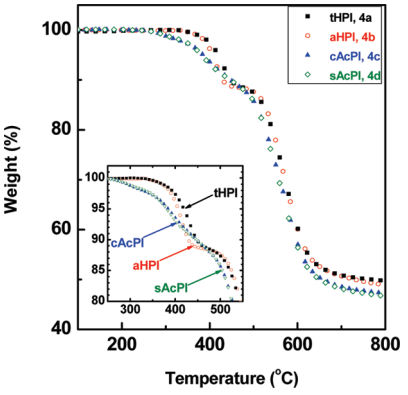

Figure 5. Thermogravimetric analysis (TGA) of precursor polyimides.

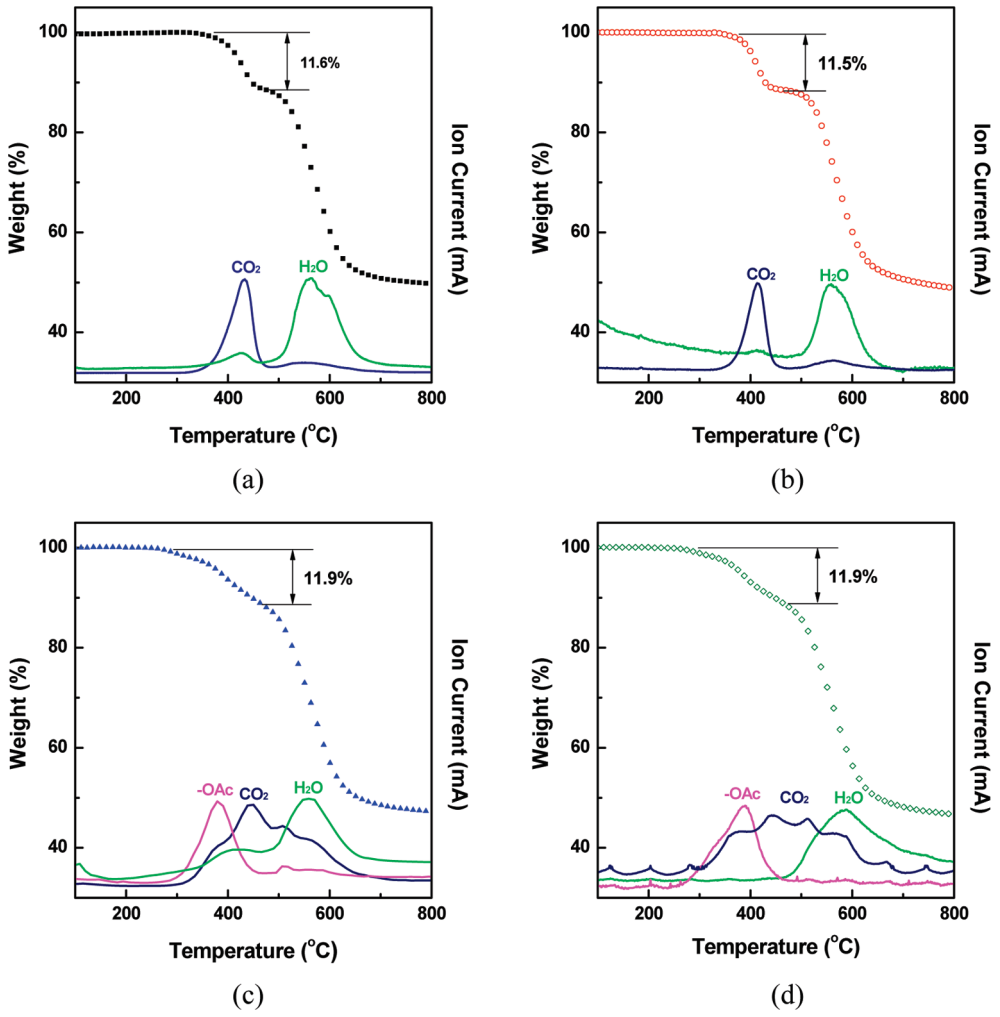

Figure 6. Thermogravimetric analysis combined with mass spectroscopy (TG-MS) of precursor polyimides: (a) tHPI (**4a**), (b) aHPI (**4b**), (c) cAcPI (**4c**), and (d) sAcPI (**4d**).

polymer structures, molecular weights, and solubilities in organic solvents. Comparing HPIs prepared from four different imidization methods, average *d*-spacing indicating the interchain distance in polymer **4a** was 0.57 nm, slightly higher than the 0.54 nm of the linear and soluble polyimide **4b** (Figure 3). This matches with the density measurements and fractional free volume (FFV) calculation for the two HPIs. The smaller density of the polymer corresponds to larger free volume elements. Note that tHPI exhibited a density of 1.47 g cm^{-3} and a FFV of 0.19, as compared with a density of 1.49 g cm^{-3} and a FFV of 0.17 in aHPI. We assumed that tHPI should have been accompanied by thermal cross-linking during thermal imidization. However, the cross-linking did not provide any change in molar volume calculation from group contribution theory. A smaller difference in free volume elements in aHPI obviously resulted from strong intermolecular forces in the soluble polyimide chains, as evidenced by the smaller *d*-spacing of aHPI (0.54 nm), as compared with that of tHPI (0.57 nm). Moreover, the incorporation of bulky acetate group displayed a decrease in density to 1.45 and 1.42 g cm^{-3}, indicating that the larger domain in the side chain made the interchain distances larger which played a role as spacers between the polyimide backbones. Although the deviation between densities of PIs from four different methods did not seem to be substantial, these changes in properties will have an impact on thermal rearrangement into the resulting polybenzoxazoles, as discussed in the following section.

Thermal Rearrangement of Polyimides into Polybenzoxazoles. Before thermal treatment, thermal behaviors of PI precursors were investigated by DSC and TGA-MS to understand thermal conversion characteristics and to set up proper thermal treatment conditions. DSC measurement revealed that the glass transition temperature (T_g) of AcPIs are 30 °C lower than those of other HPIs (Figure 4) because the large acetate moiety, which acts as a flexible spacer, allowing more rotational free energy. On the other hand, there was no distinct deviation of T_g[37] due to the thermal cross-linking between **4a** and **4b** or molecular weight between **4c** and **4d**.

Thermogravimetric analysis with simultaneous mass spectroscopy displayed thermal stabilities and provided evidence for thermal rearrangement behavior. By tracing the weight drop between 300 and 500 °C before carbonization of the main chain and matching this with the emitted molecules from mass spectroscopy at the same time (Figures 5 and 6), it is possible to elucidate what happened during thermal rearrangement.[24] As the thermal rearrangement was well demonstrated[15,16,22] in the case of tPBO (**5a**) and aPBO (**5b**), thermograms indicated two clear weight drops: a thermal rearrangement with an evolution of CO_2 confirmed by the mass number 44 at 350−450 °C and a carbonization at 500−650 °C. Different from HPIs, thermograms of AcPIs

(**5c** and **5d**) showed broad weight drop from 280 to 450 °C. At around 300 °C, the mass number 59, which signified the loss of an acetate group associated with ring fusing to the imide moiety, was detected prior to the appearance of mass number 44, which reflects thermal rearrangement with CO_2 evolution. Although the conversion rate of each precursor is not exactly the same between samples from the four different imidization methods, identical thermal treatment conditions were adopted for all the polymers to obtain conversion at 450 °C for 1 h without them undergoing deformation or carbonization at higher temperatures.

Characterization of Thermally Rearranged Polybenzoxazole (TR-PBO) Membranes. After thermal treatment in a muffle furnace at 450 °C, light yellowish precursor films turned brown or dark brown due to the charge transfer complexes (CTCs) based on the conjugation of π-bonds in polybenzoxazoles.[38,39] We could not detect the glass transition temperature (T_g) of TR-PBOs in the range of 100−500 °C, which implies that the main chain in the polyimide is converted to a highly stiff backbone rigid-rod structure with very high torsional energy. With respect to dimensional stability, PBOs from AcPIs showed 10−11% shrinkage, which was much higher than 5−6% in PBOs from HPIs due to the lower T_g of AcPIs and the evolution of larger molecules upon heating.

The resultant PBOs by thermal rearrangements of polyimides were confirmed by solid state ^{13}C NMR and elemental analysis. Because of the poor solubilities of TR-PBOs in common organic solvents, such as NMP, DMAc, and THF, ^{13}C NMR was performed rather than ^{1}H NMR. Although imide carbon peaks at 168 ppm did not remain, significant bands corresponding to aromatic benzoxazole carbons were detected at 162 and 108 ppm in all TR-PBOs, as shown in Figure 7.[40] In elemental analyses, the mass ratio of each element showed good correspondence within a small deviation compared to calculated values from the molecular formula of PBO (Table 3). The results of structural characterization signified thermal rearrangement into PBO. The PBOs derived by the diverse preparation methods had, in fact, different thermal conversion ratios for the same thermal treatment conditions. In this work, we focus on the effect of diverse imidization methods on the performances of TR-PBOs. The effect of thermal treatment conditions on the rearrangement ratio will be discussed in a subsequent paper.

TR-PBOs exhibited considerable differences in physical properties. Note that the intermolecular distances for all TR polymers increased dramatically as indicated by comparing the WAXD data of PBOs in Figure 8 with those of PIs in Figure 3. The *d*-spacing values of PBOs were in the range of 0.64−0.75 nm, except that of 0.58 nm in aPBO which was thermally rearranged from aHPI via azeotropic imidization resulting in a soluble polyimide with high intermolecular hydrogen bonds. The values of PBOs from AcPIs were higher than those of PBOs from HPIs due to the inherently wider chain distances and weaker intermolecular forces. The *d*-spacing of 0.75 nm in **5d** is comparable to those of recently reported highly permeable microporous polymers such as PIMs and fluorinated polymers except PTMSP which has a *d*-spacing of 0.93 nm.[41−43]

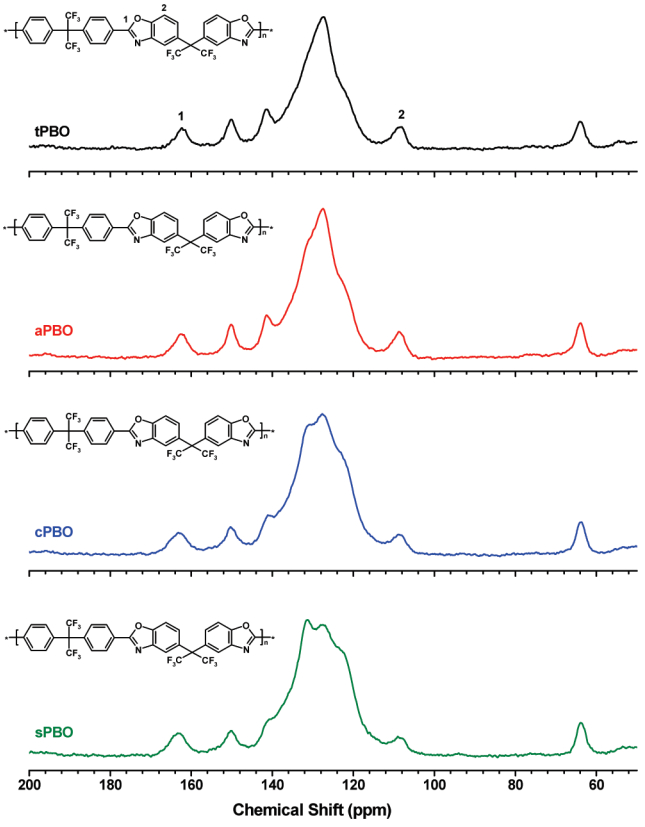

Figure 7. Solid state ^{13}C NMR spectra of polybenzoxazole membranes.

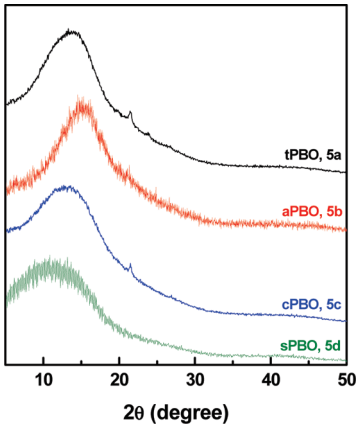

Figure 8. Wide-angle X-ray diffraction (WAXD) patterns of polybenzoxazole membranes.

Table 3. Elemental Analysis of Precursor Polyimides and Polybenzoxazole Membranes

	molecular formula of repeating unit	C (wt %)	H (wt %)	N (wt %)	total (wt %)
4a (tHPI)[a]	$C_{34}H_{14}N_2O_6F_{12}$	53.2 (52.73)*	1.87 (1.82)*	3.62 (3.62)*	58.69 (58.17)*
4b (aHPI)	$C_{34}H_{14}N_2O_6F_{12}$	51.70 (52.73)*	1.58 (1.82)*	3.73 (3.62)*	57.01 (58.17)*
4c (cAcPI)	$C_{38}H_{18}N_2O_8F_{12}$	52.44 (53.16)*	1.95 (2.11)*	3.31 (3.26)*	57.70 (58.54)*
4d (sAcPI)	$C_{38}H_{18}N_2O_8F_{12}$	52.48 (53.16)*	1.66 (2.11)*	5.03 (3.26)*	59.17 (58.54)*
5a (tPBO)[a]	$C_{32}H_{14}N_2O_2F_{12}$	56.7 (55.99)*	1.93 (2.06)*	4.21 (4.08)*	62.84 (62.13)*
5b (aPBO)	$C_{32}H_{14}N_2O_2F_{12}$	57.91 (55.99)*	1.48 (2.06)*	4.11 (4.08)*	63.50 (62.13)*
5c (cPBO)	$C_{32}H_{14}N_2O_2F_{12}$	58.60 (55.99)*	1.46 (2.06)*	3.90 (4.08)*	63.96 (62.13)*
5d (sPBO)	$C_{32}H_{14}N_2O_2F_{12}$	56.36 (55.99)*	1.21 (2.06)*	3.86 (4.08)*	61.42 (62.13)*

[a] Elemental analysis was cited from previous research.[22]

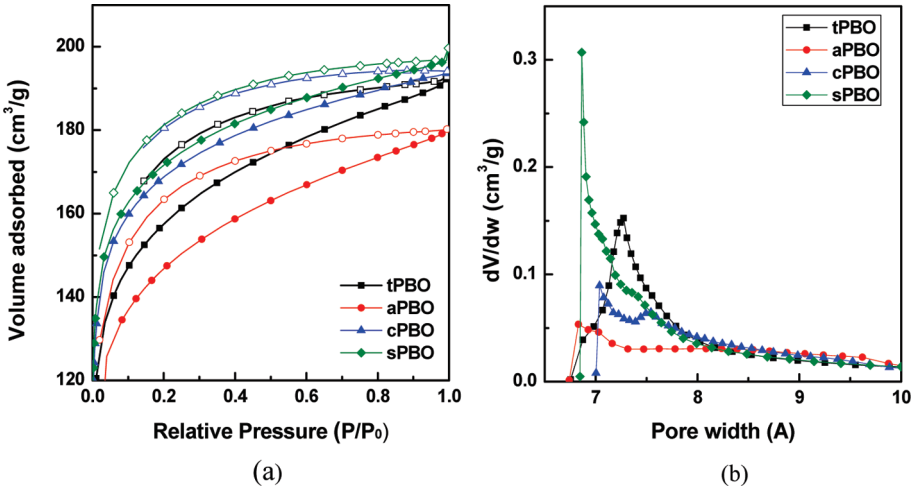

Figure 9. (a) Nitrogen adsorption/desorption isotherms of polybenzoxazoles and (b) pore size distribution by the Horvath−Kawazoe method.

Table 4. Pore Size Characterization by Positron Annihilation Lifetime Spectroscopy (PALS)

sample	τ_3 (ns)	I_3 (%)	τ_4 (ns)	I_4 (%)	cavity diameter (Å$_3$)	cavity diameter (Å$_4$)
tHPI, **4a**	2.21 ± 0.10	1.0 ± 0.2			6.08 ± 0.17	
aHPI, **4b**	2.62 ± 0.04	2.9 ± 0.1			6.73 ± 0.06	
cAcPI, **4c**	2.66 ± 0.01	7.5 ± 0.1			6.79 ± 0.01	
sAcPI, **4d**	2.71 ± 0.01	7.8 ± 0.1			6.86 ± 0.01	
tPBO, **5a**	1.24 ± 0.13	5.0 ± 0.6	5.26 ± 0.08	6.0 ± 0.2	4.04 ± 0.35	9.73 ± 0.07
aPBO, **5b**	1.06 ± 0.09	7.1 ± 0.7	3.90 ± 0.04	12.7 ± 0.7	3.51 ± 0.28	8.37 ± 0.04
cPBO, **5c**	1.01 ± 0.05	5.3 ± 0.4	5.00 ± 0.10	3.7 ± 0.1	3.35 ± 0.16	9.49 ± 0.09
sPBO, **5d**	0.94 ± 0.09	6.2 ± 1.1	4.93 ± 0.10	3.9 ± 0.1	3.12 ± 0.32	9.43 ± 0.09
PTMSP[30]	1.7	7.4	8.8	34	5.1	12.4
PMP[30]	2.3	8.4	7.6	29.4	6.2	11.6
AF 2400[30]	1.32	4.87	5.78	13.6	4.2	10.2
AF 1600[30]	1.2	5.51	5.11	17.3	3.9	9.6
PIM-1[30]	2.06	6.15	6.28	18.6	5.8	10.6

Furthermore, the increased intermolecular distances coincided with reduced densities and increased FFVs of the TR-PBOs (Table 2). Densities of the precursor polyimides were in the range of conventional glassy polymers, from 1.4 to 1.5 g cm^{-3}. As thermal rearrangements proceeded in the fluorinated polyimides, densities of TR-PBOs drastically diminished, with the exception of a milder drop in aPBO, which has the same trend in the *d*-spacing value. The FFV substantially increased from 0.19 in **4a** to 0.28 in **5a**, indicating a 48% difference between precursor and the TR-polymer.[24] Moreover, the FFVs in PBO from AcPIs which possessed higher intermolecular distances were calculated to have FFVs greater than 0.30 (FFV(**5c**) = 0.35, FFV(**5d**) = 0.33) similar to the FFV of PTMSP, the most well-known permeable organic polymers. These dramatic changes in the physical properties of TR-PBOs indicate that they may have excellent gas transport behavior and microporous characteristics.

Confirmation of Microporous Characteristics by N_2 Sorption and PALS. Nitrogen adsorption/desorption measurements at 77 K provided information on the surface area and pore volume and showed consistent trends with *d*-spacing, density, and FFV. The four isotherms of TR-PBOs showed type I behavior similar to Langmuir sorption, where type I behavior, defined by IUPAC, is common to microporous materials when the pore sizes are smaller than 2 nm (Figure 9a). There was a very broad hysteresis present in the four isotherms, while cPBO had small amounts of capillary condensation around the saturation pressure. The total pore volume of the pores was proportional to the order of Langmuir surface areas: **5d** (781.9 m^2/g) > **5c** (769.4 m^2/g) > **5a** (726.2 m^2/g) > **5b** (686.2 m^2/g). Note that all TR-PBOs show microporous characteristics with sub-nanosize cavities or free volume elements. The isotherms were similar to those of PTMSP and PIM-1, although the total adsorbed volumes of TR-PBOs were only 50−70% of those of PTMSP and PIM.[44] Nitrogen sorption measurements were performed in detail at low relative pressures (10^{-6}−10^{-2}) so that the Horvath−Kawazoe (HK) method, which is a useful method to reveal the pore size and distribution of a microporous material, could be used. As described in Figure 9b, the narrow and sharp distributions of differential pore volumes (dV/dw) for the four TR-PBOs were located in the pore width range of 6.7−7.2 Å, and the intensities had the following orders: **5d** > **5a** > **5c** > **5b**. The maximum pore widths of TR-PBOs were slightly larger than the 6.5 Å of PIM and smaller than the ∼9 Å of PTMSP, whereas the maximum dV/dw values of TR-PBOs are 1.5−4 times higher (with the exception of aPBO).[44]

Compared with *d*-spacing, density, FFVs, and nitrogen sorption, positron annihilation lifetime spectroscopy provides a more quantative measure of the size of the microcavities within the samples. Analysis of the PALS data for the PIs and TR-PBOs showed that there was one o-Ps component (τ_3) fitted for the PIs and two components (τ_3 and τ_4) for the TR-PBOs.

The low-intensity values indicate that the polyimide precursors inhibit the formation of positronium due to the strong electron affinity of the diimide moieties.[45] Thermal rearrangement of the polyimide membranes changes the 6.08 to 6.86 Å pores into a bimodal pore distribution (Table 4 and Figure 10).

Previous studies generally fit one component to untreated or unmodified polyimide materials. However, Dlubek et al. irradiated their polyimides with boron and found that a second, smaller pore cavity was formed. They assigned the 4.24 Å diameter pores to the formation of radical and unsaturated bonds as well as cross-linking and chain scission.[45] The absence of the smaller 3−4 Å cavities in the precursor materials suggests that the fluorinated polyimides may have very low gas permeabilities because the small pores are not providing interconnections between the larger 6.08−6.86 Å pores despite having FFVs of 0.18−0.19. The 3−4 Å cavities in the PBO membranes are an optimal size for selective transport of gas molecules.[46]

As a whole, these data are comparable to other classes of high free volume polymers such as PTMSP, PMP, PIM, AF 1600, and AF 2400 (Table 4). The most permeable glassy polymers—PTMSP, PMP, and PIM—have the largest τ_3 and τ_4 pores in terms of size as well as intensity. Their smaller cavities have lifetimes of more than 1.7 ns, corresponding to cavity size of 5−6 Å, which is significantly larger than the kinetic diameter of permanent gas molecules. Compared with TR-PBOs, AF 1600 and AF 2400 presented similar cavity characteristics to other glassy polymers. It is also notable that the smaller cavities with 1.2−1.3 ns lifetimes can be more selective to gas molecules as well as being highly permeable.

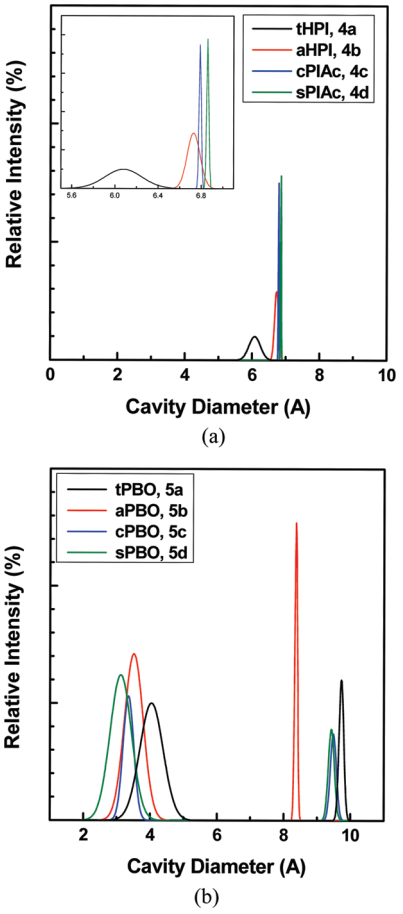

Figure 10. Cavity size analysis of (a) precursor polyimides and (b) polybenzoxazoles by positron annihilation lifetime spectroscopy (PALS).

Gas Transport Behaviors of TR-PBO Membranes. Gas permeation properties in glassy polymers are known to be dependent upon distribution and size of free volume elements.

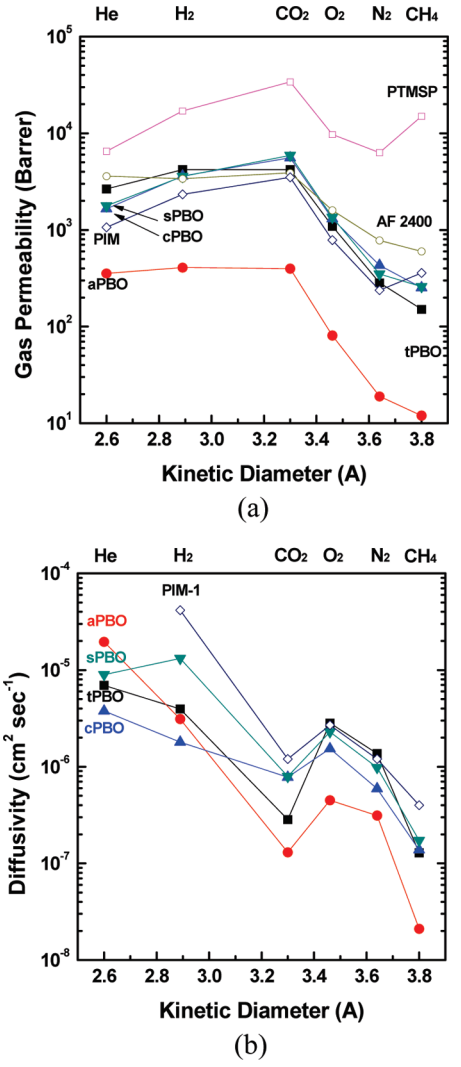

Figure 11. (a) Gas permeation properties and (b) diffusion coefficients of TR-PBOs and highly permeable polymers (■: tPBO (**5a**); ●: aPBO (**5b**); ▲: cPBO (**5c**); ▼: sPBO (**5d**); □: PTMSP;[47] ○: AF 2400;[48] ◇: PIM-1[30]).

Table 5. Gas Permeation Properties of Polybenzoxazole Membranes and Highly Permeable Glassy Polymers

	gas permeability						ideal selectivity[a]					
	He	H_2	CO_2	O_2	N_2	CH_4	O_2/N_2	CO_2/N_2	CO_2/CH_4	CO_2/H_2	H_2/CH_4	N_2/CH_4
tPBO	2647	4194	4201	1092	284	151	3.8	15	28	1.0	28	1.9
aPBO	356	408	398	81	19	12	4.3	21	34	1.0	35	1.6
cPBO	1656	3612	5568	1306	431	252	3.0	13	22	0.65	14	1.7
sPBO	1775	3585	5903	1354	350	260	3.9	17	23	0.61	14	1.4
PTMSP[47]	6500	17000	34000	9700	6300	15000	1.5	5.4	2.3	0.51	1.1	0.42
PMP[47]	2600	5800	11000	2700	1300	2900	2.1	8.5	3.8	0.53	2.0	0.45
AF 2400[48]	3600	3400	3900	1600	780	600	2.1	5.0	6.5	0.87	5.7	1.3
PIM-1[30]	1061	2332	3496	786	238	360	3.3	14.7	9.7	0.67	6.5	0.66

[a] Ideal selectivities were obtained by the ratio of two gas permeabilities.

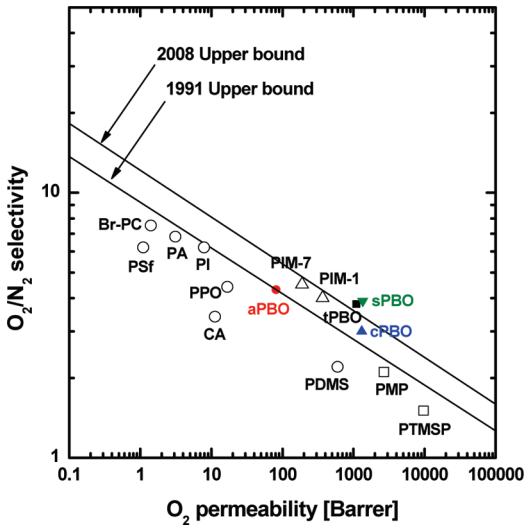

Figure 12. Relationship between O_2 permeability and O_2/N_2 selectivity of TR-PBO membranes with polymeric upper bounds.[49,50]

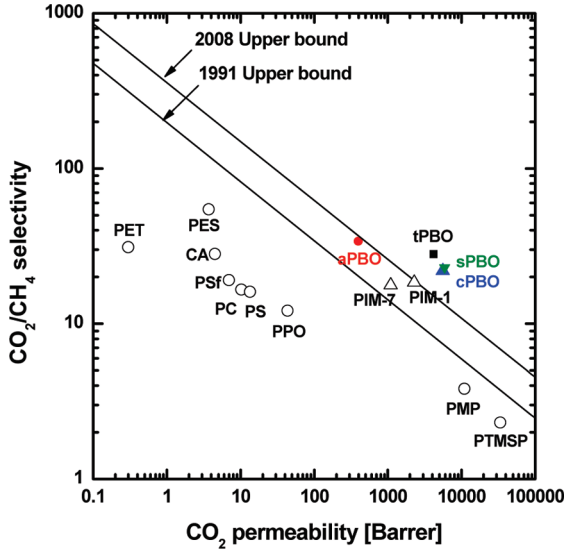

Figure 13. Relationship between CO_2 permeability and CO_2/CH_4 selectivity of TR-PBO membranes with polymeric upper bounds.[49,50]

Although precursor PI membranes had very poor permeabilities similar to conventional fluorinated polyimides, TR-PBO membranes showed high gas permeabilities due to the enlarged cavity size and distribution. Table 5 and Figure 11a show the permeation properties of TR-PBOs and representative highly permeable glassy polymer membranes. On the basis of fast diffusion rates through microcavities in TR-PBOs, as well as high sorption capacities from large surface area and pore volumes, TR-PBO membranes exhibited superior gas permeabilities for small gas molecules like He (kinetic diameter: 2.6 Å), H_2 (2.89 Å), CO_2 (3.3 Å), O_2 (3.46 Å), N_2 (3.64 Å), and CH_4 (3.8 Å). Furthermore, the ideal selectivities for binary gas mixtures, such as O_2/N_2, CO_2/N_2, and CO_2/CH_4, were close to or beyond the so-called upper bound lines. These superior performances were supported by the fact that cavity sizes of τ_3 = 3.1−4.04 Å analyzed by PALS provided efficient channels for separation of these gas molecules.[46] No remarkable difference in gas permeation was observed for cPBO and sPBO, whereas tPBO and aPBO displayed significant differences. For PBOs derived from AcPIs, CO_2 permeabilities were slightly higher than H_2 permeabilities due to higher CO_2 solubilities, originating from the large surface area and FFVs in comparison with PBOs from HPIs, where H_2/CO_2 selectivities are ~1.0. As expected by the *d*-spacing, density, FFVs, nitrogen sorption, and PALS results, gas permeabilities of aPBO were much smaller than those of other TR-PBOs. The CO_2 permeabilities of TR-PBOs are 4201 (**5a**), 398 (**5b**), 5568 (**5c**), and 5903 barrer (**5d**) while CO_2/CH_4 selectivities were between 22 and 34. These values are much higher than those of PTMSP and PIM, which showed that CH_4 permeability exceeded N_2 permeability due to the higher CH_4/N_2 sorption selectivities. On the other hand, diffusion selectivities of CO_2 and N_2 over CH_4 of TR-PBOs are dominant so high gas selectivities over CH_4 can be obtained (Figure 11b). Thus, diffusion through TR-PBOs leads to high permselectivity for permanent gas molecules. Therefore, the resultant TR-PBO membranes exhibited outstanding performance surpassing polymeric upper bounds for gas separation membranes, as shown in Figures 12 and 13.

Conclusions

Polybenzoxazole membranes were prepared by thermal rearrangement of polyimides containing ortho-functional groups. With respect to the imidization methods, different structures of precursor polyimides were synthesized, and their physical properties were characterized by ATR/FT-IR, H NMR, WAXD, density, FFVs, nitrogen sorption, and PALS. Thermal and azeotropic imidization introduced hydroxyl-containing polyimides, whereas chemical imidization formed acetate-containing polyimides. The bulky side chain in AcPIs gave rise to the change in free volume elements as well as interchain distances in the polymer matrix. In thermal rearrangement, acetate−polyimides underwent deformation of the acetate domain prior to decarboxylation, while hydroxyl−polyimides experienced a structural change directly into polybenzoxazole with decarboxylation. The intrinsic differences in the precursor polyimides resulted in significant deviations in free volume elements, although various precursors had the same structure of polybenzoxazole. PBO from azeotropic hydroxyl−polyimide without any cross-linking represented the highest density and lowest free volume elements compared with other kinds of PBOs. Cavity size and intensity of the PBOs were similar to other highly permeable glassy polymers, such as PIM and AF 2400, and proved to have high gas permeation properties. CO_2 permeability of the resulting sPBO reached 5900 barrer, and the CO_2/CH_4 selectivity was 23.

Acknowledgment. This research was supported by a grant (2009K000673) from the Carbon Dioxide Reduction & Sequestration Research Center, one of 21st Century Frontier R&D Programs funded by the Ministry of Education, Science and Technology (MEST) of the Korean Government. The project was also supported through the OCE Science Leader scheme at CSIRO.

References and Notes

(1) Ghosh, M. K.; Mittal, K. L. *Polyimides: Fundamentals and Applications*; CRC Press: Boca Raton, FL, 1996.
(2) Paul, D. R.; Yampolskii, Y. P. *Polymeric Gas Separation Membranes*; CRC Press: Boca Raton, FL, 1993.
(3) Bogert, M. T.; Renshaw, R. R. *J. Am. Chem. Soc.* **1908**, *30*, 1135–1144.
(4) Ohya, H.; Kudryavtsev, V. V.; Semenova, S. I. *Polyimide Membranes: Applications, Fabrications and Properties*; Kodansha Ltd.: Tokyo, 1996.
(5) Koros, W. J.; Fleming, G. K.; Jordan, S. M.; Kim, T. H.; Hoehn, H. H. *Prog. Polym. Sci.* **1988**, *13*, 339–401.
(6) O'brien, K. C.; Koros, W. J.; Husk, G. R. *J. Membr. Sci.* **1988**, *35*, 217–230.
(7) Paulson, G. T.; Clinch, A. B.; McCandless, F. P. *J. Membr. Sci.* **1983**, *14*, 129–137.

(8) Park, J. Y.; Paul, D. R. *J. Membr. Sci.* **1997**, *125*, 23–39.
(9) Liu, Y.; Wang, R.; Chung, T.-S. *J. Membr. Sci.* **2001**, *189*, 231–239.
(10) Low, B. T.; Xiao, Y.; Chung, T. S.; Liu, Y. *Macromolecules* **2008**, *41*, 1297–1309.
(11) Ghanem, B. S.; McKeown, N. B.; Budd, P. M.; Al-Harbi, N. M.; Fritsch, D.; Heinrich, K.; Starannikova, L.; Tokarev, A.; Yampolskii, Y. *Macromolecules* **2009**, *42*, 7881–7888.
(12) Weber, J.; Su, Q.; Antonietti, M.; Thomas, A. *Macromol. Rapid Commun.* **2007**, *28*, 1871–1876.
(13) Guo, X.; Fang, J.; Watari, T.; Tanaka, K.; Kita, H.; Okamoto, K. I. *Macromolecules* **2002**, *35*, 6707–6713.
(14) Fang, J.; Kita, H.; Okamoto, K. I. *J. Membr. Sci.* **2001**, *182*, 245–256.
(15) Tullos, G. L.; Powers, J. M.; Jeskey, S. J.; Mathias, L. J. *Macromolecules* **1999**, *32*, 3598–3612.
(16) Tullos, G. L.; Mathias, L. J. *Polymer* **1999**, *40*, 3463–3468.
(17) Yu, D.; Gharavi, A.; Yu, L. *Macromolecules* **1995**, *28*, 784–786.
(18) Ding, Y.; Bikson, B.; Nelson, J. K. *Macromolecules* **2001**, *35*, 905–911.
(19) Likhatchev, D.; Gutierrez-Wing, C.; Kardash, I.; Vera-Graziano, R. *J. Appl. Polym. Sci.* **1996**, *59*, 725–735.
(20) Muñoz, D. M.; De La Campa, J. G.; De Abajo, J.; Lozano, A. E. *Macromolecules* **2007**, *40*, 8225–8232.
(21) Muñoz, D. M.; Calle, M.; de la Campa, J. G.; de Abajo, J.; Lozano, A. E. *Macromolecules* **2009**, *42*, 5892–5894.
(22) Park, H. B.; Jung, C. H.; Lee, Y. M.; Hill, A. J.; Pas, S. J.; Mudie, S. T.; Wagner, E. V.; Freeman, B. D.; Cookson, D. J. *Science* **2007**, *318*, 254–258.
(23) Han, S. H.; Lee, J. E.; Lee, K.-J.; Park, H. B.; Lee, Y. M. *J. Membr. Sci.* **2010**, *357*, 143–151.
(24) Park, H. B.; Han, S. H.; Jung, C. H.; Lee, Y. M.; Hill, A. J. *J. Membr. Sci.* **2010**, *359*, 11–24.
(25) Tao, S. J. *J. Chem. Phys.* **1972**, *56*, 5499–5510.
(26) Eldrup, M.; Lightbody, D.; Sherwood, J. N. *Chem. Phys.* **1981**, *63*, 51–58.
(27) Rudel, M.; Kruse, J.; Rätzke, K.; Faupel, F.; Yampolskii, Y. P.; Shantarovich, V. P.; Dlubek, G. *Macromolecules* **2008**, *41*, 788–795.
(28) Merkel, T. C.; He, Z.; Pinnau, I.; Freeman, B. D.; Meakin, P.; Hill, A. J. *Macromolecules* **2003**, *36*, 6844–6855.
(29) Dlubek, G.; Pionteck, J.; Rätzke, K.; Kruse, J.; Faupel, F. *Macromolecules* **2008**, *41*, 6125–6133.
(30) Staiger, C. L.; Pas, S. J.; Hill, A. J.; Cornelius, C. J. *Chem. Mater.* **2008**, *20*, 2606–2608.
(31) Choi, J. I.; Jung, C. H.; Han, S. H.; Park, H. B.; Lee, Y. M. *J. Membr. Sci.* **2010**, *349*, 358–368.
(32) Omote, T.; Koseki, K.; Yamaoka, T. *Macromolecules* **1990**, *23*, 4788–4795.
(33) Omote, T.; Mochizuki, H.; Koseki, K.; Yamaoka, T. *Macromolecules* **1990**, *23*, 4796–4802.
(34) Maruyama, Y.; Oishi, Y.; Kakimoto, M. A.; Imai, Y. *Macromolecules* **1988**, *21*, 2305–2309.
(35) Pavia, D.; Lampman, G.; Kriz, G. *Introduction to Spectroscopy*, 3rd ed.; Brooks Cole: Salt Lake City, UT, 2001.
(36) Foord, E. K.; Cole, J.; Crawford, M. J.; Emsley, J. W.; Celebre, G.; Longeri, M.; Lindon, J. C. *Liq. Cryst.* **1995**, *18*, 615–621.
(37) Wind, J. D.; Staudt-Bickel, C.; Paul, D. R.; Koros, W. J. *Macromolecules* **2003**, *36*, 1882–1888.
(38) Hariharan, R.; Sarojadevi, M. *J. Appl. Polym. Sci.* **2006**, *102*, 4127–4135.
(39) Natori, I.; Natori, S.; Ogino, K. *Macromolecules* **2009**, *42*, 1964–1969.
(40) Chang, J. H.; Park, K. M.; Lee, S. M.; Oh, J. B. *J. Polym. Sci., Part B: Polym. Phys.* **2000**, *38*, 2537–2545.
(41) Du, N.; Robertson, G. P.; Song, J.; Pinnau, I.; Thomas, S.; Guiver, M. D. *Macromolecules* **2008**, *41*, 9656–9662.
(42) Alentiev, A. Y.; Yampolskii, Y. P.; Shantarovich, V. P.; Nemser, S. M.; Platé, N. A. *J. Membr. Sci.* **1997**, *126*, 123–132.
(43) Masuda, T.; Isobe, E.; Higashimura, T. *Macromolecules* **1985**, *18*, 841–845.
(44) Budd, P. M.; Msayib, K. J.; Tattershall, C. E.; Ghanem, B. S.; Reynolds, K. J.; McKeown, N. B.; Fritsch, D. *J. Membr. Sci.* **2005**, *251*, 263–269.
(45) Dlubek, G.; Buchhold, R.; Hubner, C.; Nakladal, A.; Sahre, K. *J. Polym. Sci.,Part B: Polym. Phys.* **1999**, *37*, 2539–2543.
(46) Thornton, A. W.; Hilder, T.; Hill, A. J.; Hill, J. M. *J. Membr. Sci.* **2009**, *336*, 101–108.
(47) Park, H. B.; Lee, Y. M. Polymeric Membrane Materials and Potential Use in Gas Separation. In *Advanced Membrane Technology and Applications*; Li, N. N., Fane, A. G., Ho, W. S. W., Matsuura, T., Eds.; Wiley: Hoboken, New Jersey, 2008; pp 633−669.
(48) Pinnau, I.; Toy, L. G. *J. Membr. Sci.* **1996**, *109*, 125–133.
(49) Robeson, L. M. *J. Membr. Sci.* **1991**, *62*, 165–185.
(50) Robeson, L. M. *J. Membr. Sci.* **2008**, *320*, 390–400.